Recurrent Rossby waves and South-eastern Australian heatwaves

S. Mubashshir Ali*[1], Matthias Röthlisberger[2], Tess Parker[3], Kai Kornhuber[4], and Olivia Martius[1,5]

1. Oeschger Centre for Climate Change Research and Institute of Geography, University of Bern, Bern, Switzerland,
2. Institute for Atmospheric and Climate Science, ETH Zürich, Zürich, Switzerland,
3. School of Earth, Atmosphere and Environment, Monash University, Clayton VIC, Australia,
4. Earth Institute, Columbia University, New York City, NY, USA, and
5. Mobiliar Lab for Natural Risks, University of Bern, Bern, Switzerland.

*Corresponding author: mubashshir.ali@giub.unibe.ch

Abstract

In the Northern Hemisphere, recurrence of transient Rossby wave packets over periods of days to weeks, termed RRWPs, may repeatedly create similar surface weather conditions. This recurrence can lead to persistent surface anomalies. Here, we first demonstrate the significance of RRWPs for persistent hot spells in the Southern Hemisphere (SH) using the ERA-I reanalysis dataset and then examine the role of RRWPs and blocks for heatwaves over south-eastern Australia (SEA).

A Weibull regression analysis shows that RRWPs are statistically associated with a significant increase in the duration of hot spells over several regions in the SH, including SEA. Two case studies of heatwaves in SEA in the summers of 2004 and 2009 illustrate the role of RRWPs in forming recurrent ridges (anticyclonic potential vorticity, PV anomalies), aiding in the persistence of the heatwaves. Then, using an observation-based dataset to identify SEA heatwaves, we find that SEA heatwaves are more frequent than climatology during days with extreme RRWPs activity. On days with both RRWPs and heatwaves, a circumglobal zonal wavenumber 4 anomaly pattern is present in the upper-level PV field, with an anticyclonic PV anomaly over SEA. In addition, we find positive blocking frequency anomalies over the Indian and the south Pacific Oceans, which may help to modulate the phase of RRWPs during SEA heatwaves.

1. Introduction

Since 1900, extreme heat has been responsible for more fatalities in Australia than all other natural hazards combined (Coates et al., 2014). Heatwaves also exacerbate the risk of wildfires, cause surges in power demand, and increase insurance costs (Hughes et al., 2020; Insurance Council of Australia, 2020). Increasingly frequent and severe heatwaves in the midlatitudes in the recent years (Coumou et al., 2013; Perkins-Kirkpatrick and Lewis, 2020; IPCC 2021) have spurred fruitful research on the atmospheric drivers of heatwaves. Understanding the dynamical mechanisms is particularly important for improving sub-seasonal prediction (Quandt et al., 2017) and for quantifying future changes in heatwaves (Shepherd, 2014; Wehrli et al., 2019). Several large-scale atmospheric mechanisms and phenomena have been identified as potential drivers of heatwaves in the Northern Hemisphere extra-tropics. They include blocking anticyclones (e.g., Barriopedro et al., 2011; Drouard and Woollings, 2018, Kautz et al., 2021), amplified quasi-stationary waves (Teng et al., 2016; Kornhuber et al., 2017), amplified Rossby wave patterns (e.g., Fragkoulidis et al., 2018; Kornhuber et al., 2020), and recurrent Rossby wave patterns (Röthlisberger et al., 2019). Fragkoulidis et al. (2018) showed that amplified Rossby waves are correlated with surface temperature extremes over NH and used process-based understanding to establish further association for the 2003 and 2010 NH heatwaves. RRWPs can be considered as a subset of amplified Rossby waves with a condition that the transient eddies recur spatially in the same phase on a short time scale of days to weeks. Here, we focus on recurrent Rossby wave patterns to explore their importance for heatwaves in south-eastern Australia (SEA).

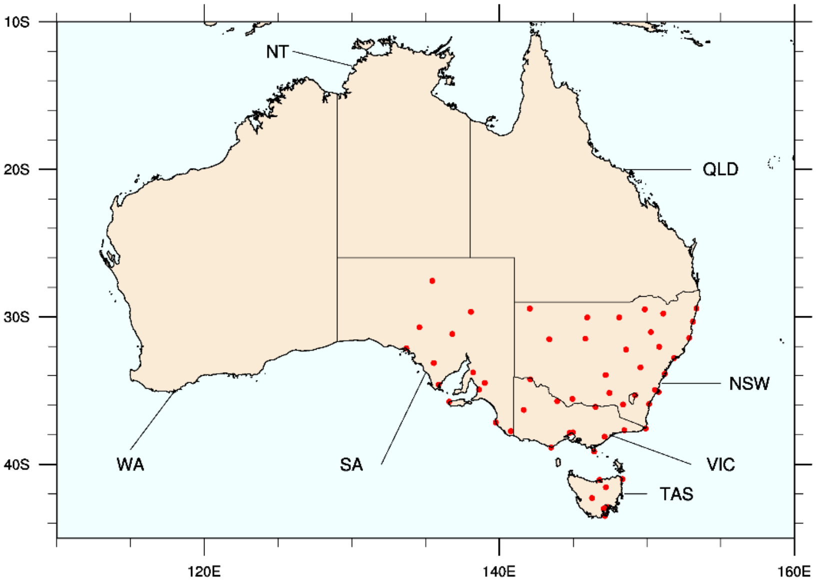

Figure 1. Map of Australia showing the states of South-eastern Australia (SEA): South Australia (SA), Tasmania (TAS), Victoria (VIC), and New South Wales (NSW). Other states shown are Queensland (QLD), Northern Territory (NT), and Western Australia (WA). Red dots indicate Australian Bureau of Meteorology's (BoM) monitoring stations used in this study (see Methods).

Broadly, heatwaves in SEA (Fig. 1), comprising the states of Victoria (VIC), New South Wales (NSW), South Australia (SA), and Tasmania (TAS), are associated with slow-moving transient anticyclonic upper-level potential vorticity (PV) anomalies over the Tasman Sea (e.g., Marshall et al., 2013; Parker et al., 2014a; Quinting and Reeder, 2017; Parker et al., 2019). The anticyclonic PV anomalies and the associated subsidence drive heatwaves over VIC (Parker et al., 2014b; Quinting and Reeder, 2017). These anticyclonic PV anomalies can form as a part of synoptic-scale Rossby wave packet (RWP) (King and Reeder, 2021). These RWPs are often initiated several days before the onset of the heatwaves, but they amplify, and eventually break over SEA as anticyclonic equatorward (LC1-type) Rossby wave breaking (Parker et al., 2014a; O'Brien and Reeder, 2017).

Surface temperature anomalies associated with transient RWPs form, amplify, and decay on synoptic timescales, but the recurrence of RWPs in the same phase on a sub-seasonal timescale can result in persistent surface weather conditions by repeatedly re-enforcing the surface temperature anomalies (e.g; Hoskins and Sardeshmukh, 1987; Davies, 2015). Röthlisberger et al. (2019) termed this phenomenon "Recurrent Rossby wave packets" (RRWPs) and demonstrated a statistically significant connection between RRWPs and the persistent of surface temperature anomalies in the Northern Hemisphere (NH). Ali et al. (2021) found that RRWPs are also associated with increased persistence of dry and wet spells in several regions across the globe.

However, at least for some impacts, it is not only the simple occurrence of an extreme, however one defines an extreme, but also the duration of the extreme event that is important. This study addresses that aspect for the temperature extremes in the SH. More precisely, we evaluate the hypothesis whether an increase in R-metric, a measure of RRWPs (Röthlisberger et al. 2019), is associated with an increase in spell duration of the surface-temperature extremes over SH. Furthermore, we show how SH RRWPs relate to the persistent and extreme SEA heatwaves and demonstrate their association with the help of two case studies for the 2004 and 2009 heatwaves.

2. Methods

2.1 Data

This study uses ERA-Interim (ERA-I) reanalysis data (Dee et al., 2011) provided by the European Centre for Medium-Range Weather Forecasts on a 1° × 1° spatial grid for 1979–2018. Various fields are used including horizontal velocity, meridional velocity, 2 m temperature, PV, and sea surface temperature (SST). The datasets are freely available to download from https://apps.ecmwf.int/datasets/data/interim-full-daily/levtype=pl/. The PV fields in the SH are multiplied by a factor of -1. The climatological mean is calculated with respect to the period 1980–2010.

2.1 Recurrent Rossby Waves

The metric *R*, developed by Röthlisberger et al. (2019), is used identify recurrence of synoptic-scale Rossby wave patterns. For the SH, we use the same metric as in Ali et al. (2021). First, a 14.25 day running mean of meridional velocity fields ($\hat{v}_{tf}(\lambda, t)$), averaged between 35° S and 65° S, are calculated to isolate signals with timescales longer than the synoptic timescale for each longitude λ and time *t*. The envelope of the synoptic wavenumber contribution to the time-filtered *v* is extracted following Zimin et al., (2003). To do this, the time-filtered *v* fields are transformed into the frequency domain using a fast Fourier transform over longitude, $\hat{v}_{tf}(k, t)$. Finally, an inverse Fourier transform is applied to calculate the envelope of the wave while only considering contributions from a selected band of synoptic wavenumbers *k* = 4–15. Thus, $R(\lambda, t)$ for each longitude λ and time t is calculated as

$$R(\lambda, t) = \left| 2 \sum_{k=4}^{k=15} \hat{v}_{tf}(k, t) e^{2\pi i k l_\lambda / N} \right| \quad (1)$$

where k is the wavenumber, l_λ denotes the longitudinal grid point index for longitude λ and $N = 360$ denotes the number of longitudinal grid points.

In most cases, large values of *R* reliably identify situations in which amplified waves (of distinct wave packets) recur in the same phase. However, the definition of *R* does not contain criterion for recurrence of distinct wave packets. Thus, in a few cases, high values of *R* over a few days may result from stationary synoptic-scale troughs or ridges (see Röthlisberger et al. 2019 for discussion on metric *R*). Fig. A1 shows day-of-year climatology of the *R* metric in the Southern Hemisphere and compares it to that of the Northern Hemisphere. The code for calculating R metric is freely available (check Code and data availability section).

Phase and amplitude information of a particular wavenumber k can also be extracted using the same technique as in (1) and presented by Zimin et al. (2003). After applying the inverse Fourier transform, a complex number of the form $a + ib$ is obtained. For extracting the wave packet or envelop, the amplitude of the complex number is taken as shown in (1). Instead of that, plotting the complex number on a complex plain provides information on the phase and amplitude at a given time step t for a particular wavenumber k. This is used to obtain a phase-amplitude distribution shown later.

2.2 Atmospheric blocks

Atmospheric blocks are identified from persistent anticyclonic PV anomalies averaged between 500 hPa and 150 hPa vertical levels with the detection scheme described in Schwierz et al. (2004) as updated by Rohrer et al. (2018). The code used is available on GitHub (https://github.com/marco-rohrer/TM2D). The detection scheme uses a 1.3 PVU threshold, a persistence criterion of 5 days, and a minimum overlap of 0.7 between two timesteps. Blocking fields identified with this algorithm are available at 6 hourly temporal resolution and 1° × 1° spatial resolution. We tested the sensitivity of the blocking fields with a 1.0 PVU threshold for the two case studies and did not find blocking directly over SEA.

2.3 South-eastern Australian Heatwaves

A station-based heatwave dataset is used to focus on extreme and persistent heatwaves in SEA to study the links between RRWPs, blocks, and QRA conditions. Following the methods developed in Parker et al. (2014a) and refined in Quinting and Reeder (2017), heatwaves in SEA in December–February (DJF) are detected from temperatures observed at the Australian Bureau of Meteorology's (BoM) monitoring stations (Fig. 1). The BoM's Australian Climate Observations Reference Network – Surface Air Temperature (ACORN-SAT, available at *http://www.bom.gov.au/climate/data/acorn-sat/#tabs=ACORN%E2%80%90SAT*) is a high-quality temperature dataset used to monitor long-term temperature trends. The dataset provides a daily maximum temperature (TMAX) for each station. These TMAXs are extracted for stations in SEA as defined here, for DJF from 1979 to 2019. The 90th percentile TMAX (T90) is then calculated for each station for each month in DJF. A heatwave is defined as any period of at least four consecutive days for which the TMAXs at three or more of these stations equal or exceed the T90 for that station and month. From here on, the term “heatwave” refers to heatwave in SEA. This criterion results in 57 heatwaves, which were on an average 8 days long with the longest heatwave lasting 22 days. Note that the purpose of the heatwave identification scheme is to identify the most intense and most persistent heatwaves in SEA, and thus serves a different purpose than the hot spell identification scheme described in the next section. Following Parker et al. 2014a, a day part of the SEA heatwaves is termed as SEA heat day. For evaluating the co-occurrence of SEA HD with RRWP conditions, high R_{SEA} days are defined as days exceeding the 90th percentile of the daily mean R averaged over SEA (between 130° E and 153° E). The 90th percentile threshold is a subjectively chosen threshold consistent with the threshold for TMAX. Sensitivity test with a threshold of 85th percentile did not change the conditional probability shown in section 3.3.

2.4 Hot Spells in the SH

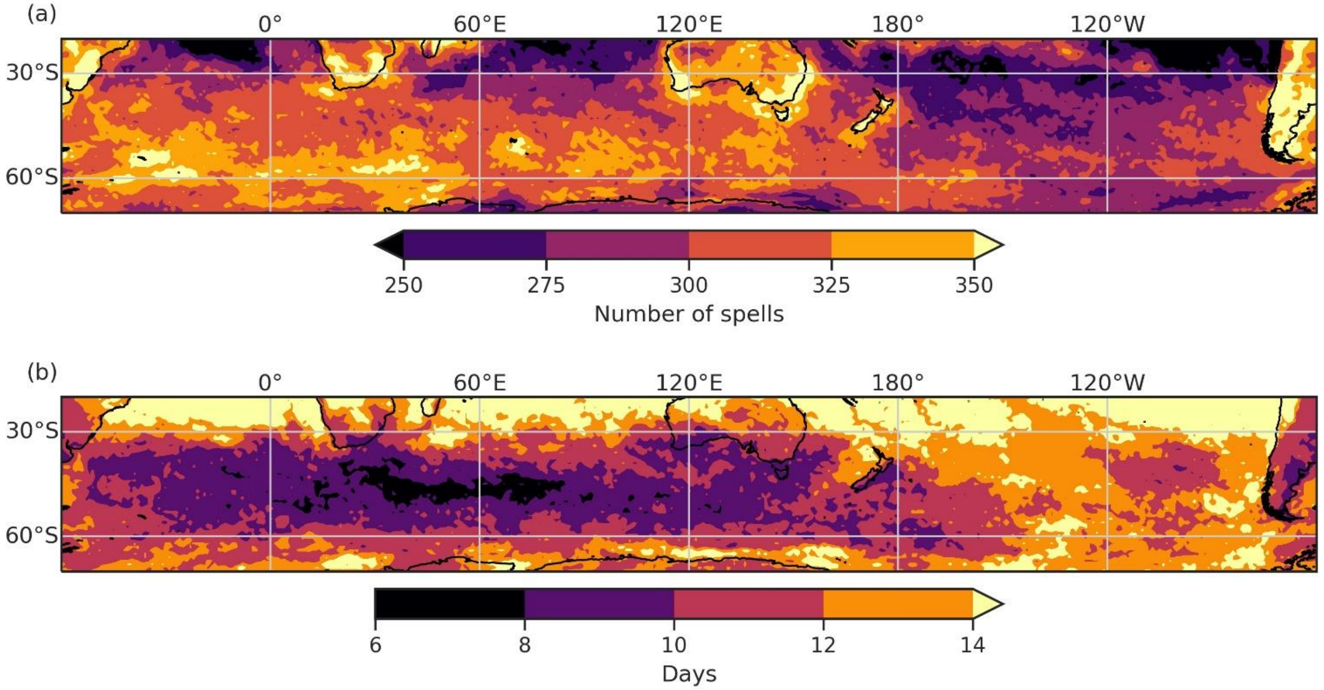

Figure 2: (a) Total number of hot spells in November–April identified at each grid point between 20° S and 70° S. (b) The 95th percentile of hot spell durations.

Hot spells are identified for all SH grid points between 20°S and 70°S for 1980–2016 using 2 metre temperatures (T2M) from the ERA-I fields at 6 hourly temporal resolution and 1-degree spatial resolution. The hot spells definition follows that of Röthlisberger et al. (2019), in which a hot spell is calculated for each grid point as consecutive values exceeding the 85th percentile from the linearly detrended T2M fields. Spells separated by less than a day are merged to form a single uninterrupted spell. Spell durations of less than 36 hours are excluded from further analysis. Contrary to the SEA heatwave identification scheme, the purpose of the hot spell identification scheme is to identify many (not necessarily overly extreme) warm periods at each grid point, which can then be used for statistical analyses of the factors that determine the duration of these events. This statistical analysis (see next section) will be used to quantify the effect of RRWPs on the persistence of warm surface weather. To ensure a large sample size for robust statistical results, we identify hot spells for the period of November to April. Figure 2a shows the spatial distribution of the number of hot spells at each grid point between 20° S and 70° S. Higher number of hot spells are seen over land where parts of SEA, South Africa, and South America show 350 or more spells. The 95th percentile for hot spell duration varies from 6 days to more than 2 weeks (Fig. 2b). Over SEA, the 95th percentile duration varies from a week to roughly 2 weeks.

2.5 Weibull regression model to assess the effect of RRWPs in the SH hot spells

To quantify the effect of RRWPs on the persistence of hot surface weather, we extend an analysis from Röthlisberger et al. (2019) to the SH, including SEA, using the same statistical model setup, a Weibull regression model. This model allows us to model the distribution of the duration of hot spells at each grid point. An advantage of Röthlisberger et al.'s (2019) model is that we do not need to subjectively define the duration of a significant spell because the model accounts for the assessment of changes in all quantiles of the spell duration modelled. The null hypothesis tested here is that RRWPs have no effect on the duration of hot spells, which is tested at each grid point. The Weibull model is only briefly introduced here. Please refer to Röthlisberger et al. (2019) for further details and their Supporting Information for a detailed introduction to the Weibull model.

To fit the Weibull model to the observed spell duration, a representative value of the R-metric needs to be assigned to each hot spell. This is achieved in the following way: for each hot spell i at grid point g with a duration $D_{g,i}$, the raw R metric

$R(\lambda, t)$ is longitudinally averaged within a 60° longitudinal sector centred at the grid point g with longitude λ_g to yield $R_{lon}(\lambda, \mathrm{t})$. Then, a median of $R_{lon}(\lambda, \mathrm{t})$ is calculated for the lifetime of the hot spell to assign a representative value of R $(\tilde{R}_{\lambda_g,i})$ for each spell. Thus, our model is given as:

$$\ln\left(D_{g,i}\right) = \alpha_{0,g} + \alpha_{1,g}\tilde{R}_{\lambda_g,i} + \sum_{j=2}^{6} \alpha_{j,g} m_j\left(t_{g,i}^{start}\right) + \sigma_g \epsilon_{g,i} \quad ; i = 1, \dots n_g. \qquad (2)$$

Hereby $\alpha_{0,g}$ is the intercept, $\alpha_{1,g}$ is the regression coefficient for $\tilde{R}_{\lambda_g}$ and the $\alpha_{j,g}$ are regression coefficients for dummy variables $m_j\left(t_{g,i}^{start}\right)$ that take the value 1 if spell i starts in month m_j, and zero otherwise. The coefficients $\alpha_{j,g}$, therefore, account for possible seasonality in the spell duration distribution at grid point g (e.g., longer hot spells in May compared to, e.g., September), while σ_g is a scale parameter and the $\epsilon_{g,i}$ are error terms. The quantity $\exp(\alpha_1)$ is usually referred to as acceleration factor (*AF*) and is of particular interest here, as it quantifies the factor of change in all quantiles of the distribution of spell duration at grid point g per unit increase in $\tilde{R}$ (Hosmer et al., 2008; Zhang, 2016; Röthlisberger et al., 2019). An *AF* >1 implies an increase in all spell duration quantiles with increasing $\tilde{R}$ (i.e., during RRWPs), and conversely for an *AF* <1. Furthermore, fitting the model (2) to spell durations at all grid points thus results in a spatial field of *AF*. The statistical significance of the *AF* values is evaluated in a two-step approach. First, a p-value for the above null hypothesis is computed exactly as in Zhang (2016). Then, the false-discovery-rate (FDR) test of Benjamini and Hochberg, (1995) is applied to the resulting field of p-values. The FDR test controls for type I errors, i.e., falsely rejecting null hypothesis that can occur substantially in analyses like this one where multiple tests are being performed independently from each other at each grid point (e.g., Wilks 2016). Here we follow the recommendation of Wilks (2016) and allow for a maximum false-discovery-rate α_{FDR} of 0.1.

This model is fitted to durations of hot spells at each grid point. It results in a spatial field of regression coefficients $\alpha_{j,g}, j = 0, \dots, 6$, together with their p values. Here, $\alpha_{1,g}$ represents the effect of $\tilde{R}$ on the hot spell duration. The $\exp(\alpha_1)$, referred to as the acceleration factor (*AF*), corresponds to the factor of change in all quantiles of the spell duration D per unit increase in $\tilde{R}$ (Hosmer et al., 2008; Röthlisberger et al., 2019; Zhang, 2016). Statistical significance of *AF* is evaluated after controlling the false discovery rate (FDR) (Benjamini and Hochberg, 1995) for type I errors due to falsely rejecting null hypothesis in multiple independent tests by setting the FDR threshold, α_{FDR} to 0.1 as recommended by Wilk's (2016). Thus, regions with AF >1 (AF<1) experience an increase (decrease) in spell duration with increasing (decreasing) R.

3. Results

3.1 RRWPs and hot spell durations

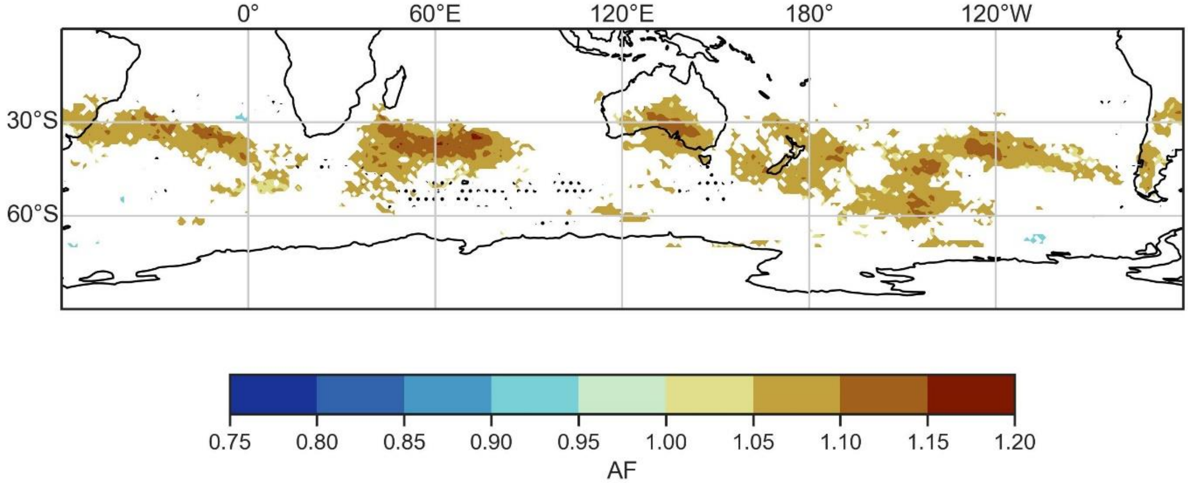

Figure 3: Statistically significant acceleration factors (AF) for hot spells in November–April between 20° S and 70° S. Colours show AFs from a Weibull model with R metric as a covariate. Stippling indicates grid points where spell durations do not follow the Weibull model based on the Anderson–Darling test at a significance level of 0.01.

The Weibull analysis reveals that RRWPs are significantly correlated with the duration of hot spells in several regions within the SH and including over SEA (Fig. 3). Recall that AF larger than 1 means that an increase in R is related to an increase in hot spell duration and conversely for AF smaller than 1. Thus, several parts of central and southern Australia, including the states of SA, VIC, NSW, and TAS, experience longer hot spells during periods when RRWPs occur. Northern Australia, however, does not show such a correlation with RRWPs, which agrees with previous studies showing different dynamical pathways for Northern and Southern Australian heatwaves (Risbey et al., 2017; Quinting and Reeder, 2017; Parker et al., 2019). Other statistically significant areas over land include parts of South America: southern Brazil, Bolivia, and parts of Argentina and Chile. For Northern Hemisphere summer half-year, the significant AFs, larger than 1, form a wavenumber 7 pattern (Röthlisberger et al., 2019). In contrast, no clear wave pattern emerges for the SH in the significant AFs in Fig. 3.

The difference in AF patterns between the two hemispheres is consistent with different climatological stationary wave patterns. The spatial pattern in Figure 3 highlights areas where the transient waves building up the RRWPs have a predominant phasing in summer. In summary, the regression analysis shows that RRWPs are significantly associated with the duration of hot spells in several SH regions over land, including SEA. However, the Weibull analysis does not provide any information about the processes and hence potential causal link between RRWPs and the most intense SEA heatwaves. Accordingly, we next focus on SEA heatwaves and elucidate the role of RRWPs and blocks for two selected cases studies of SEA heatwaves and investigate further co-occurrence of SEA heatwaves and days with high *R* activity.

3.2 RRWPs, Blocks. and QRA during two extreme and persistent SEA heatwaves

3.2.1 Case 1: 2004 Heatwave

The February 2004 heatwave (7–22 February) lasted for 16 days. More than 60% of continental Australia recorded temperatures above 39°C during this event (National Climate Centre, 2004). At the time, this event was the most severe February heatwave on record in both spatial and temporal extent and ranked in the top five Australian heatwaves for any month (National Climate Centre, 2004). More than 100 stations in SA, NSW, and northern VIC experienced record temperatures for February, and in some regions all-time records were set for consecutive days of heat (BoM, 2004). Previous studies have shown that the upper-level anticyclonic PV anomalies over SEA during the heatwaves are associated with subsidence and is the major process causing the high surface temperature anomalies (e.g., Quinting and Reeder, 2017; Parker et al., 2019). The surface flow associated with anticyclonic anomalies may also advect warm continental air due to the north westerly flow at lower levels (e.g., Parker et. al. 2014b). Here, we show how RRWPs contribute to persistent anticyclonic PV anomalies over SEA.

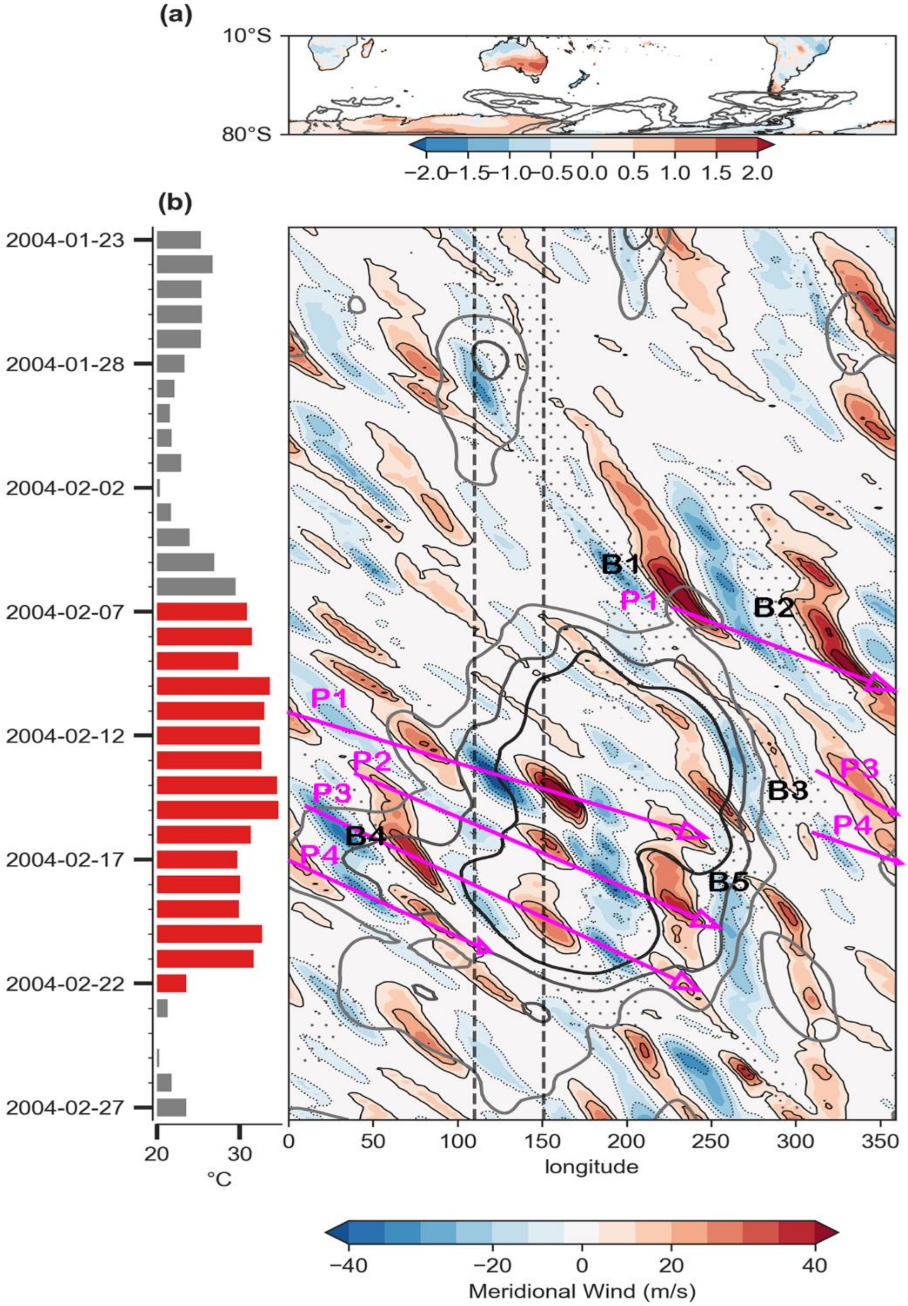

Figure 4: RRWPs, and blocks during 2004 SEA heatwave. (a) Filled contours depict the time-mean standardized anomalies of daily maximum 2 m temperature over land for the duration of the heatwave. Contours show the mean blocking frequency during the heatwave (5, 10, 20%). (b) Bars show daily maximum 2 m temperature averaged over SEA (°C); red marks the heatwave period. The Hovmöller diagram shows the meridional wind at 250 hPa averaged between 35° S and 65 °S (filled contours, m/s), *R* values (grey contours, 6, 8, 10 m/s), and longitudes at which at least one grid point between 40° S and 70° S featured an atmospheric block (stippling). Rossby wave packets (blocks) are labelled in magenta (black).

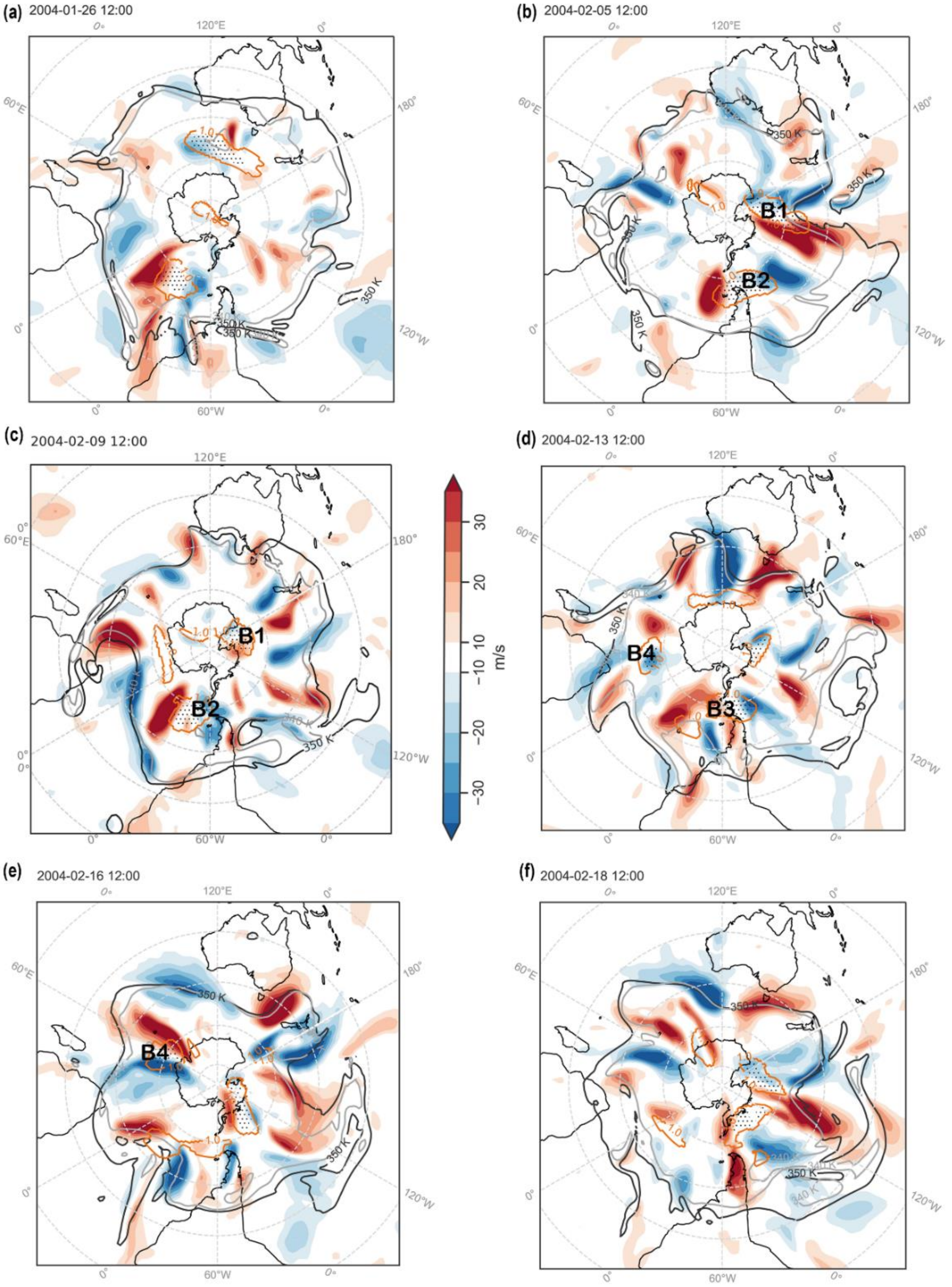

Figure 5: (a), (b), (c), (d), (e), and (f) show meridional velocity at 250 hPa (colour shading), 2 PVU contours at isentropes 340 K (black line) and 350 K (grey line) at various time steps. Stippling and orange contours show blocks identified using a 1.3 and 1.0 PVU threshold, respectively.

During this event, several Rossby wave packets were observed, recurrently amplifying in the same phase forming a ridge over SEA. The upper-level flow over SEA was zonal prior to the heatwave (Fig. 5a). An upper-level ridge forms over SEA around 5 February prior to the heatwave (Fig. 5b). The flow becomes more amplified in the subsequent days with a circumglobal amplified wave pattern apparent around 9 February (Fig. 5c). The amplified wave, part of a transient and nonstationary Rossby wave packet, RWP (P1 in Fig. 4b), arrived over the southern Indian Ocean, and an upper-level ridge began to form over Australia which amplified further around 13 February (Fig 5c). Two further ridges formed over SEA on 16 and 18 February (Fig. 5e, 5f), each ridge being part of a transient nonstationary RWP initiated upstream of Australia (P3, P4 in Fig 5b). These series of upper-level recurrent ridges were part of the RRWPs and contributed to the persistence of the heatwave. These recurrent ridges associated with RRWPs were also detected by the metric *R* (grey contours in Fig. 4b).

No blocks were identified directly over SEA during the heatwave, but blocks were present south of SEA and further downstream (Fig. 4, 5). The RWP labelled as P1 in Figure 5b formed downstream of a block B1 downstream of Australia where the block moved from south of Australia a few days earlier (Fig. 5b). Another block B2 was simultaneously present in the vicinity of South America around 7 February. In the next few days, simultaneous wave breaking was observed in the central Pacific Ocean and south of Africa in the Indian Ocean. Another set of RWPs (P3 and P4 in Fig. 4b) seems to have been set off by a block over the Pacific Ocean (B3 in Fig. 5b). Simultaneously, another block was present south of South America (B4 in Fig. 4b, 5d), and seem to initiate another RWP (P3 in Fig. 4b). Block B4 was also associated with amplified Rossby waves downstream over the Indian Ocean on 16 February (Fig. 5d). Thus, we argue that blocks could have played a key role in the initiating, phasing, and meridional amplification of the three Rossby wave packets (P1–P4) that reached Australia between 13 and 18 February. In summary, we saw recurring RWPs that passed over Australia during this period (Fig. 4b). These waves were not stationary, they were not triggered in the same area, and not over Australia, and were initially not in phase upstream of Australia.

3.2.2 Case 2: 2009 Heatwave

The 2009 heatwave (27 January–9 February), although extensively covered in literature (e.g., Engel et al. 2013, Parker et al. 2014b), has been chosen because it is one of the most severe heatwaves in SEA. It lasted for 14 days. Between 28–31 January and 6–8 February, temperatures in SEA were exceptionally high. On Black Saturday, 7 February, the hot, dry, and windy conditions worsened many catastrophic fires in VIC, which recorded 173 fatalities, and more than 2133 houses were destroyed (Karoly 2009; Parker et al., 2014b; VBRC 2010). During this heatwave, an anticyclone over SEA and the associated north-westerly flow at the surface advected hot continental air into SEA leading to extreme surface temperatures (Parker et al., 2014b).

Prior to the onset of the heatwave, the flow was already amplified with a wave breaking over SEA (Fig. 7a). Several RRWPs were observed prior to and during this event (P1 and P2 in Fig. 6b). The RRWPs prior to the heatwave were not in the same phase as those during the heatwave (Fig. 6b). Around 26 January, a Rossby wave packet (P2 in Fig 6b) was observed forming an upper-level ridge forming over Australia (Fig. 6b, 7b). In the subsequent days, the amplified wave broke anticyclonically over SEA (Fig. 7c), resulting in an anticyclonic PV anomaly over SEA (see Parker et al., 2014 for a detailed analysis of this event). On 2 February, a new ridge started forming over southern Australia (Fig. 7c) as part of Rossby wave packet (P3 in Fig 6b) and reached over SEA on 5 February (Fig. 7d). However, the upper-level ridge was transient and was replaced by another ridge around 7 February as part of another amplified wave (P4 in Fig. 6, Fig. 7e).

No blocks were identified directly over SEA during the heatwave (Fig. 6, 7). However, blocks were frequent upstream of SEA from 50° E to 70° E in the Indian Ocean (B2 in Fig. 6b, Fig. 7), and downstream of SEA from 200° E to 250° E (B1 in Fig. 6b, 7). Block B2 over the Indian ocean was particularly persistent and interacted with several amplified Rossby wave packets (T2, T4). B2 began to weaken around 2 February (Fig. 7c) but restrengthened again on 5 February (Fig. 8d) due to injection of low PV from a smaller southward moving block in the Indian Ocean (not shown). Therefore, B2 remained persistent throughout the heatwave. Rossby wave packet P1 formed downstream of the block B1 over the Pacific Ocean prior to the heatwave (Fig 6b, 7a).

So far, we have investigated the association of RRWPs with duration of hot spells. We also presented two cases of extreme and persistent SEA heatwaves to show how RRWPs can lead to the formation or replenish the anticyclonic PV anomalies over SEA. Figure B1 shows another case of SEA heatwave associated with RRWPs. In the next section, we extend the analysis to a climatological period (1979–2018) and explore high R_{SEA} conditions for all the SEA heatwaves.

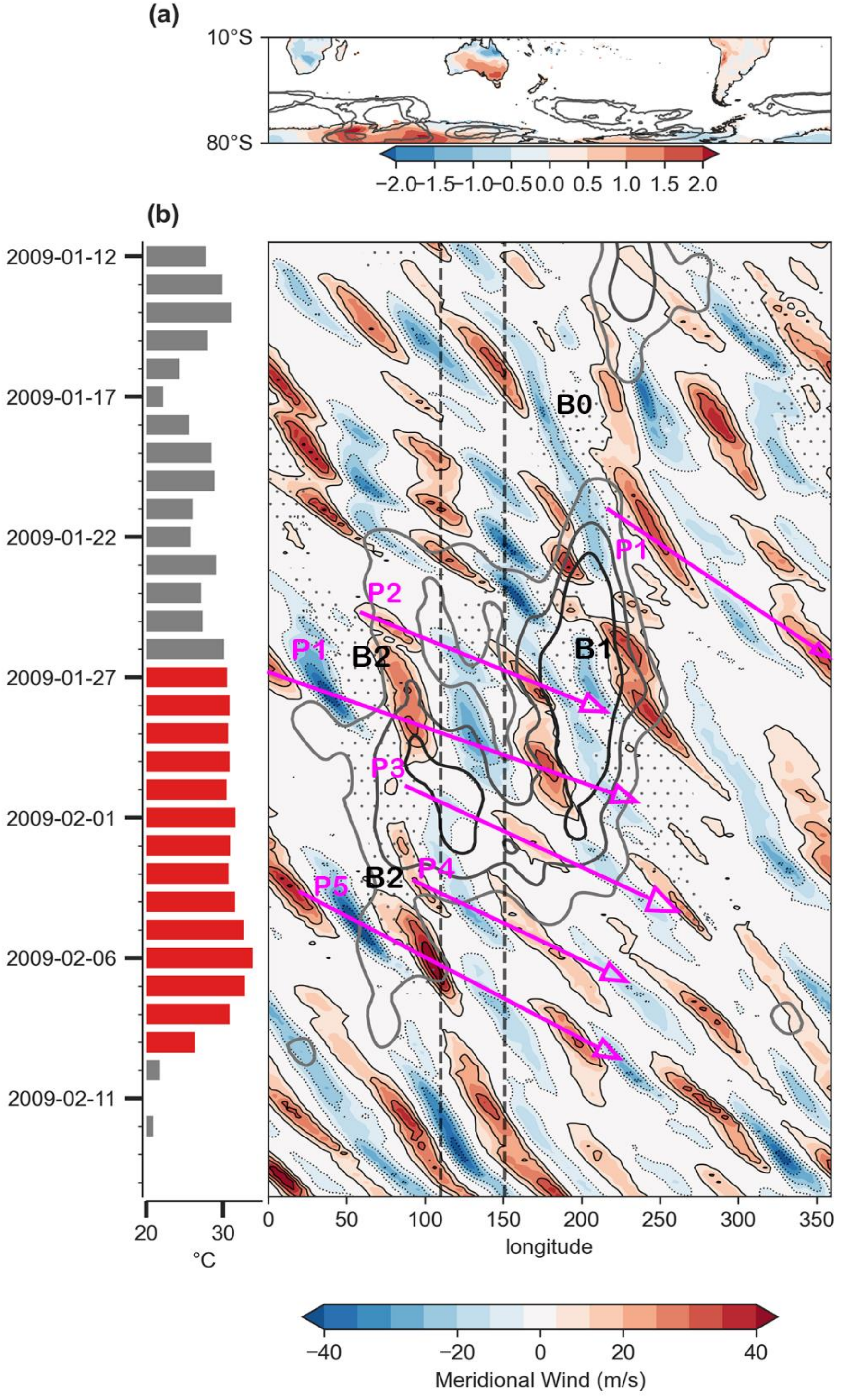

Figure 6: Same as in Fig. 4 but for February 2009 SEA heatwave.

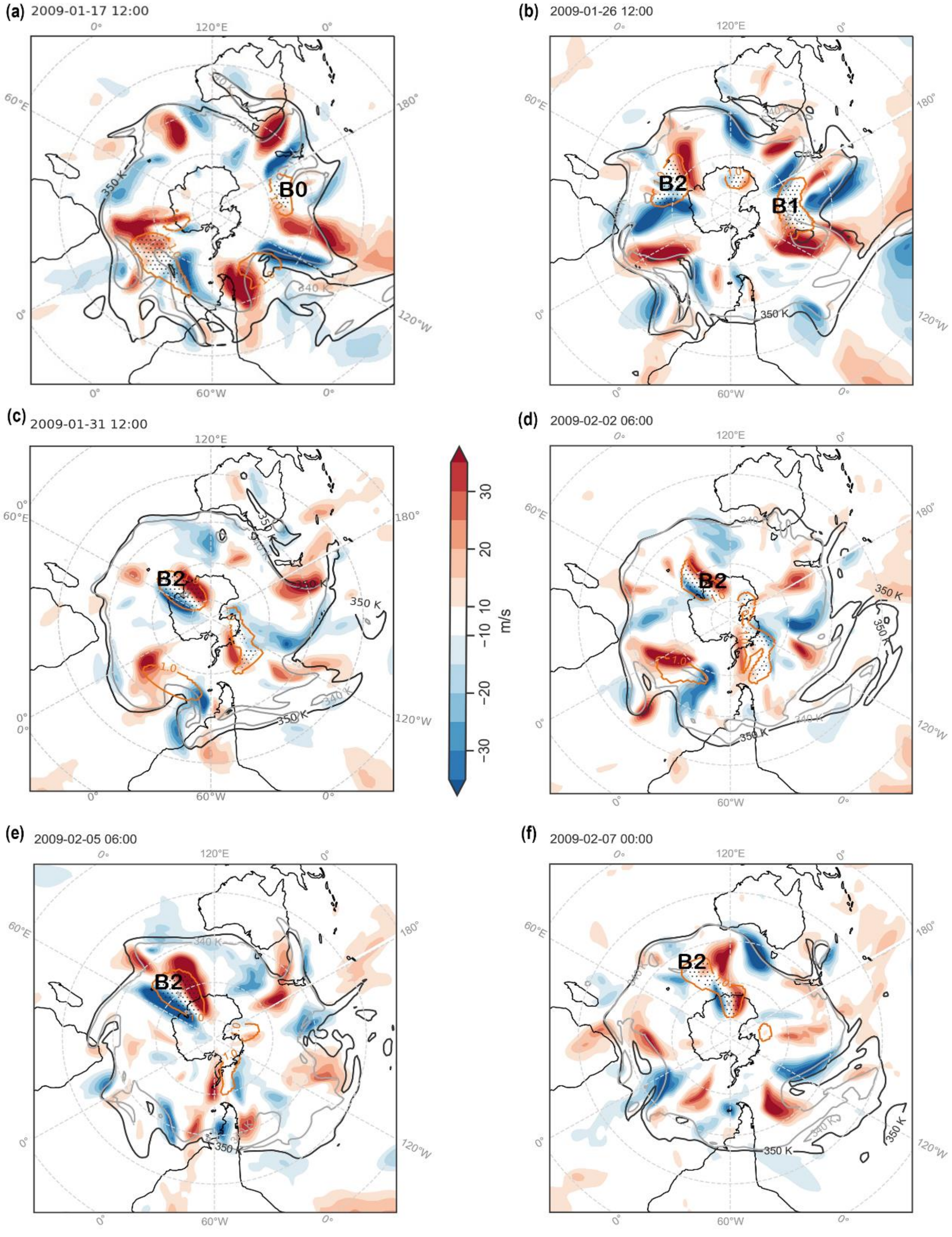

270 **Figure 7: Same as in Fig. 6 except for 2009 SEA heatwave.**

3.3 RRWP conditions during SEA heatwaves

First, a note on the co-occurrence of high R_{SEA} days and SEA heatwave days (SEA HD) as defined in section 2.3. Out of 352 days with high R_{SEA}, 67 co-occur with SEA HD and 285 do not co-occur (Table C1). Thus, the conditional probability of a SEA HD given high R_{SEA} is 0.19 (67/352=0.19), which is higher than the climatology (457/3520=0.13). Many high R_{SEA} days do not co-occur with SEA HD, which clearly indicates that R is not a sufficient condition for SEA heatwaves on its own. We, therefore, further explore that why some high R_{SEA} days co-occur with SEA HD while others do not.

High R_{SEA} days co-occurring with SEA HD feature a large anticyclonic PV anomaly over SEA (Fig. 8a) on the 350 K isentropic surface. The 2 PVU isoline on the 350 K isentropic surface, indicating the dynamic tropopause, is also located over SEA, thereby indicating a suitable choice of the isentropic surface. Upstream and downstream of the anticyclonic PV anomaly over SEA feature cyclonic PV anomalies that are also located equatorward of the highest blocking frequencies (black contours in Fig. 8a). These may correspond to the cyclonic PV anomalies surrounding omega-type blocking or the cyclonic PV anomalies of the dipole blocks. Since blocking is a binary dataset, the blocking frequency in Figures 8a and 8b indicates the percentage of days on which a grid point features a block. Thus, for high R_{SEA} days co-occurring with SEA HD, blocks are more frequent over the Indian and the south Pacific Oceans close to the Antarctic coast compared to high R_{SEA} days without co-occurring SEA HD (Fig. 8a, 8c) and less frequent over the 60° S latitude, the latitudinal band featuring high blocking frequency in the DJF climatology (Fig. 8c, 8f). In contrast, on high R_{SEA} days not co-occurring with SEA HD there is no spatial preference for the anticyclonic PV anomalies. Weak zonally elongated PV anomalies are present over the ocean basins, that are co-located with the blocking frequency fields (black contours in Fig. 8b). Near Australia, the centroid of the contour of anticyclonic PV anomaly appears around 30° downstream of SEA over New Zealand (Fig. 8b) compared to over SEA in Figure 8a. The difference in the spatial distribution of PV anomalies on the high R_{SEA} days not co-occurring with SEA HD and the high R_{SEA} days co-occurring on SEA HD suggests that only the RRWPs whose phase is conducive to forming ridges over SEA are important for SEA heatwaves.

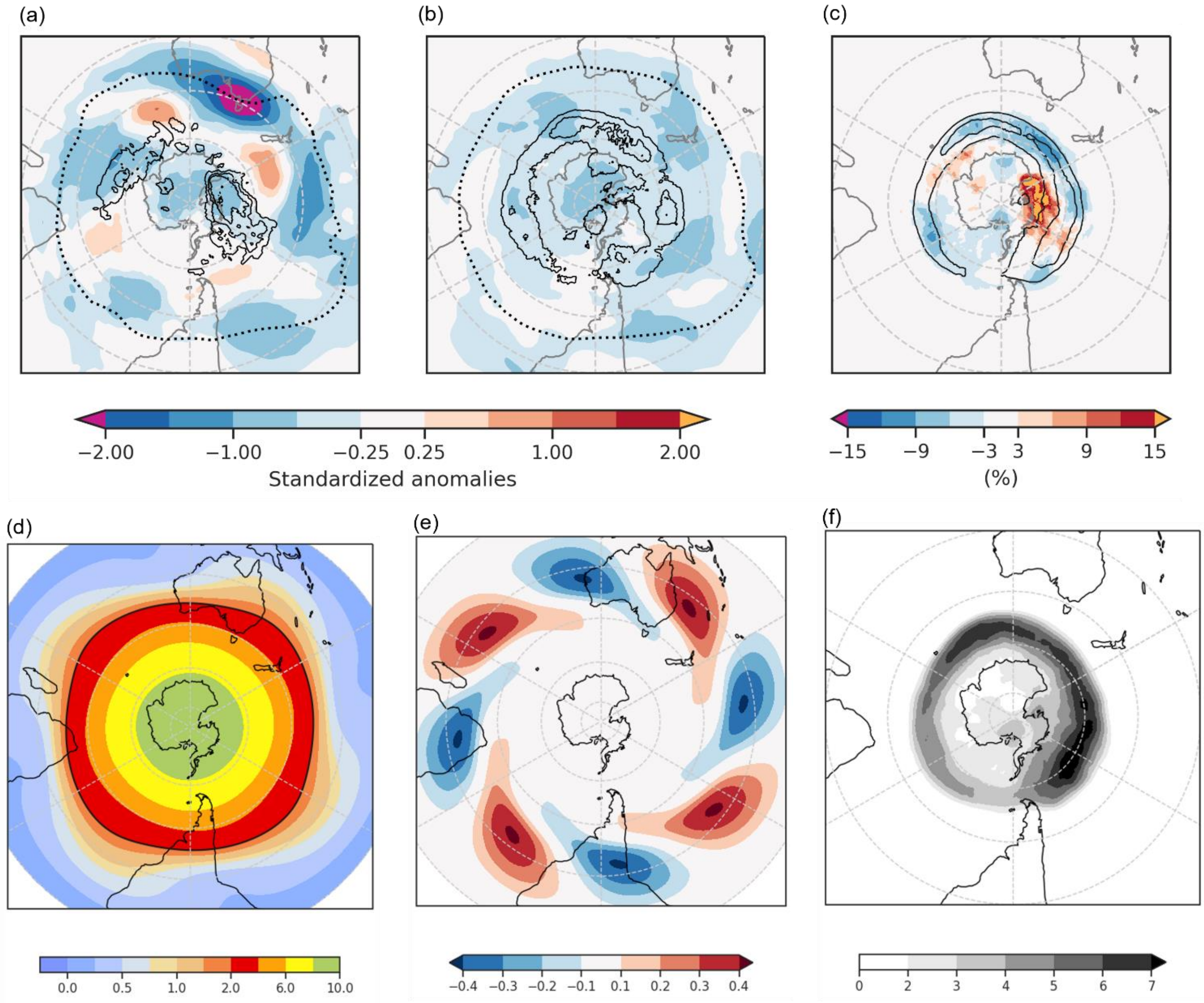

Figure 8: Standardized PV anomalies on the 350 K isentrope with respect to the DJF climatology (1979–2018) for (a) High R_{SEA} days and SEA heatwave days (HD), (b) High R_{SEA} days and non-SEA HD. Dotted black lines show 2 PVU contour in the mean PV fields for (a) and (b), and black contours show mean blocking frequency contours at 5, 10, 15 % for the same. (c) Shows the difference in blocking frequency between (a) and (b). (d) shows the sum of PV (in PVU) from the zonal wavenumber, $k = 4$ component of the DJF climatology at 350 K (shown in e) and the k=0 (the DC) component. (f) shows the climatological mean blocking frequency (%) for DJF, and black contours in (c) show the same at 4, 6%.

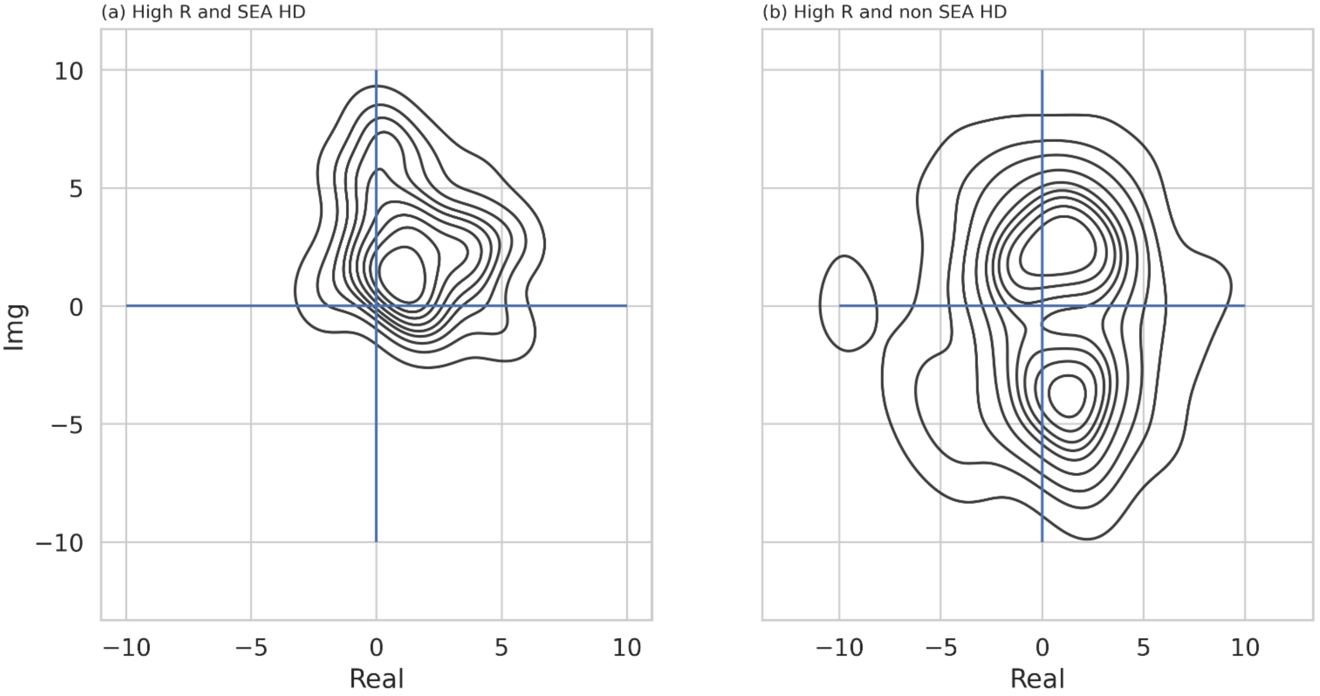

Figure 9. Bivariate kernel density estimate using Gaussian kernels in the complex plain of the Fourier decomposed meridional wind at 250 hPa averaged between 35°S and 65°S. Only zonal wavenumber 4 is shown for days belonging to (a) high R_{SEA} and SEA HD, and (b) high R_{SEA} and non-SEA HD.

In addition to the ridge over SEA, a circum-hemispheric zonal wavenumber 4 (WN4) pattern is present in the composite mean PV fields for high R_{SEA} days co-occurring on SEA HD (Fig. 8a). This WN4 pattern does not have the same distribution of PV anomalies as the WN4 extracted from the Fourier decomposition of the climatological mean PV field for DJF: the WN4 climatology features the anticyclonic PV anomaly node roughly 30° west of SEA (Fig 8d, 8e).

A high fraction of WN4 flow during high R_{SEA} days co-occurring on SEA HD is in phase (Fig. 9). Figure 9 shows the phase and amplitude density distribution of the WN4 component of the meridional winds averaged between 35° S and 65° S. Phase and amplitude information for each wavenumber can be extracted using a Fourier decomposition as shown in section 2.1. On high R and SEA HD, the density distribution in the complex plain is unimodal point to a preferred phasing of the wave that is reflected in WN4 pattern visible in the PV composite (Fig. 8a). On high R_{SEA} and SEA HD density distribution in the complex plain is bimodal and generally much broader, that agrees with the PV composite that shows no clear WN4 pattern (Fig. 8b). The phase distribution for wavenumber 4 is shown here because it emerges as the dominant pattern in the composite mean (Fig. 8a), whereas density distributions for other wavenumbers do not exhibit a clear difference (not shown). Overall, our results agree with the understanding of SEA heatwaves featuring upper-level anticyclonic PV anomalies over SEA (Marshall et al., 2013; Parker et al., 2014b; Quinting and Reeder, 2017), and we show how RRWPs in a particular phase are conducive to forming anticyclones over SEA.

4. Discussion

During the 2004 and 2009 SEA heatwaves, we find transient and fast-moving Rossby waves organized in wave packets, recurring in the same phase to form a ridge over SEA, thereby contributing to the persistence of the heatwave conditions. This persistence arises by recurrence, in contrast to the persistence arising from stationary weather features such as slow-moving Rossby waves (e.g., Wolf et al., 2018) or blocking anticyclones (e.g., Kautz et al. 2022). The Rossby wave packets observed during the two SEA heatwaves were not always initiated in the same area. In the 2004 case, these waves were mostly not in phase upstream of Australia, whereas in the 2009 case, they were also in phase upstream over the Indian Ocean. Blocks were observed upstream and downstream during the two heatwaves and suggests that blocks could play a role in initiating the RWPs and/or in modulating their phase. Figure D1 presents relationship between R anomalies and the blocks in the Indian and south Pacific Oceans for DJF. Overall, our results agree with Risbey et al. (2018) and King and Reeder (2021), who reported transient waves in the Indian Ocean preceding SEA heatwaves and transient circulation anomalies during SEA heatwaves. More specifically, we show how recurrent Rossby waves aid in the persistence of the well-known upper-level anticyclonic PV anomalies during SEA heatwaves by forming recurrent upper-level ridges.

The relevance of RRWPs for persistent SEA heatwaves documented in these two case studies is consistent with the results of the Weibull regression analysis, which reveals a significant positive statistical link between the duration of hot spells over SEA and RRWPs. PV composite for high R_{SEA} days co-occurring with SEA heatwaves shows an anticyclonic PV anomaly over SEA (Fig. 8), which is a typical feature of SEA heatwaves (Parker et al., 2014b; Quinting and Reeder, 2017). The PV composite also shows a wavenumber 4 pattern, where the anticyclonic PV anomalies are located upstream and downstream of blocking frequency maxima. Furthermore, the distribution of the zonal wavenumber in the complex plain indicates a preferred phasing for high R_{SEA} days part of SEA heatwaves (Fig. 9). The results from the Weibull regression analysis also suggests preferred phasing of the transient eddies not only over SEA but also upstream and downstream of it. Therefore, recurrent Rossby wave packets in the right phase could help to foster the anticyclonic anomalies over SEA for time periods exceeding the lifespan of an individual wave packet. Hence, the combined evidence from the literature summarized above, together with the observations from the two case studies and the results from the regression analysis, suggest a causal link between RRWPs and persistent SEA heatwaves. The proposed link works as follows: heatwaves over SEA are forced by subsidence occurring in anticyclones of SEA (e.g., Quinting and Reeder, 2017). RRWPs result in the repeated formation of these ridges over SEA and thereby contribute to the persistence of the ridges and thus, the heatwaves. However, not all SEA HD are associated with RRWPs, and hence other dynamical pathways for SEA heatwaves exist. In addition, local negative soil moisture anomalies strengthen positive temperature anomalies through increased surface sensible heat fluxes and may thereby extend the duration of heat waves (e.g., Green 1977; Seneviratne et al. 2010; Martius et al. 2021).

A reverse causal link between surface temperature anomalies during SEA heatwaves and R_{SEA} is theoretically possible, namely that the positive surface temperature anomaly contributes substantially to the upper-level ridge and that this ridge amplification increases R_{SEA}. This causal link cannot be distinguished in our Weibull model set-up. However, model experiments from Martius et al. (2021) suggest that the influence of surface temperature anomalies over Australia on the upper-level (250hPa) geopotential height and wind anomalies is quite small; therefore, the imprint on R-metric after the latitudinal averaging is even smaller.

5. Conclusions

We find that RRWPs are associated with a significant increase in the persistence of hot spells in the SH. In several parts of SEA, including the states of South Australia, New South Wales, Victoria, and Tasmania, longer hot spells coincide with high amplitude RRWPs (Fig. 3). Other regions over land where RRWPs are statistically associated with hot spell duration include South America: southern Brazil, Bolivia, and parts of Argentina and Chile.

We have demonstrated the role of RRWPs in building persistent ridges during two cases of SEA heatwaves: the 2004 and 2009 heatwaves. Both heatwaves featured RRWPs comprised of transient Rossby waves, which were in phase regionally but not hemisphere wide. Blocks were not directly observed over SEA, but the case studies suggest that blocks upstream and downstream played an important role in initiating the Rossby wave packets and modulating their phase. We further investigated the co-occurrence of RRWPs during the most persistent and extreme SEA heatwaves using the R-metric.

We find that days with R exceeding the 90th percentile, high R_{SEA} days, are associated with increased probabilities of being part of a heatwave compared to climatology. These conditional probabilities have similar magnitudes as those with remote drivers MJO, El Nino (Parker et al., 2014a). However, not all high R_{SEA} days are associated with heatwaves. Further investigations suggest that those high R_{SEA} days, that are relevant for the SEA heatwaves, play a role in forming or sustaining the ridges over SEA. Such high R_{SEA} days exhibit a circumglobal zonal wavenumber 4 pattern in the PV composite and indicate a preferred phasing of the waves. The high R_{SEA} days that do not coincide with SEA heatwave days do not show preferred phasing (a ridge or a trough) over SEA. Therefore, R accompanied with information on the phasing of the wave packets could be used as a diagnostic metric for SEA heatwaves.

The following open questions remain: what is the role of blocks in initiating RRWPs and modulating their phase? The case studies and the PV composites suggest that blocking might play an important role. What is the role of background flow in setting up RRWPs and modulating their phase? The interaction of RRWPs with other well-known climate oscillation patterns such as the El Nino-Southern Oscillation and the Southern Annular Mode also needs to be investigated further. Better understanding of the interplay between these features might offer an opportunity to improve sub-seasonal forecasts during RRWP events.

Appendix A: Comparison of *R* anomalies for Southern Hemisphere and Northern Hemisphere

Both the Southern and Northern Hemisphere *R* fields show seasonality. Anomalies are highest for Northern Hemisphere boreal autumn and winter days. Interestingly, the Southern Hemisphere shows higher *R* anomalies during austral summer days than winter days.

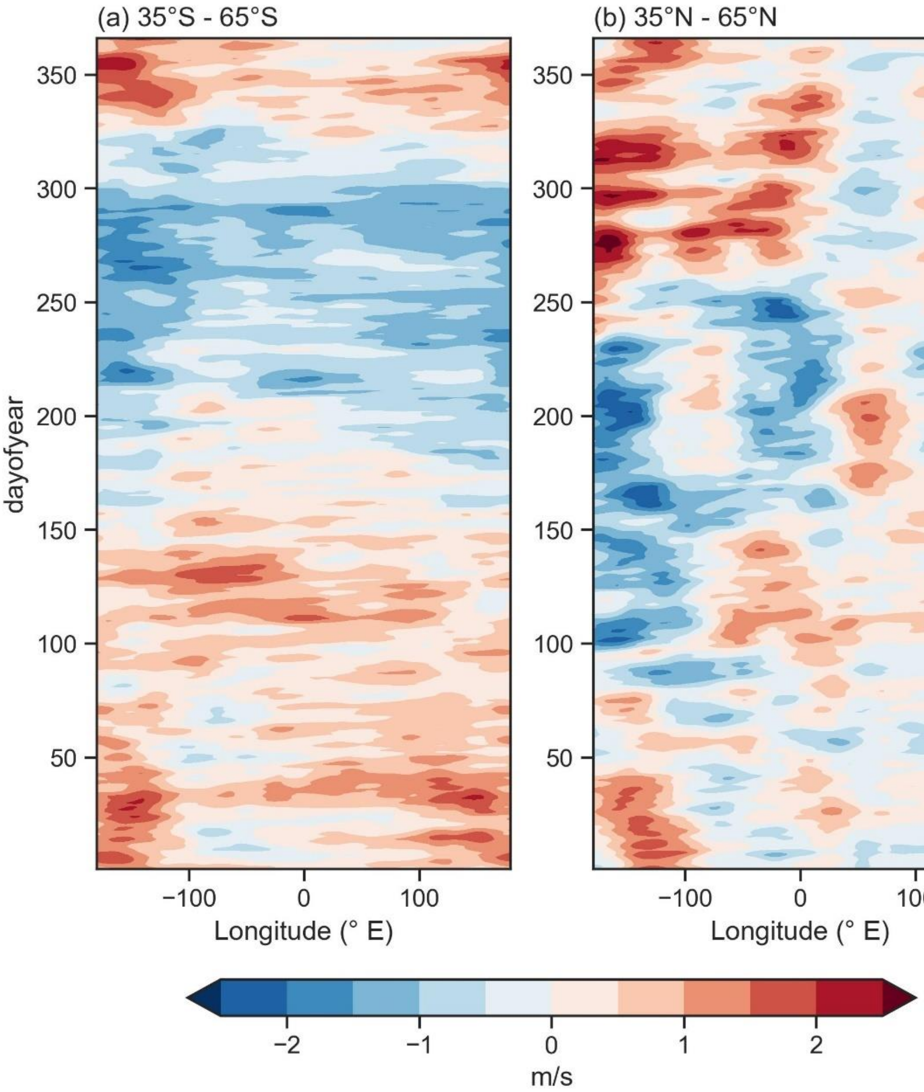

Figure A1: *R* anomalies for Southern and Northern hemispheres. Anomalies for day-of-year mean are calculated with respect to mean *R* fields.

Appendix B: RRWPs during 2014 Heatwaves

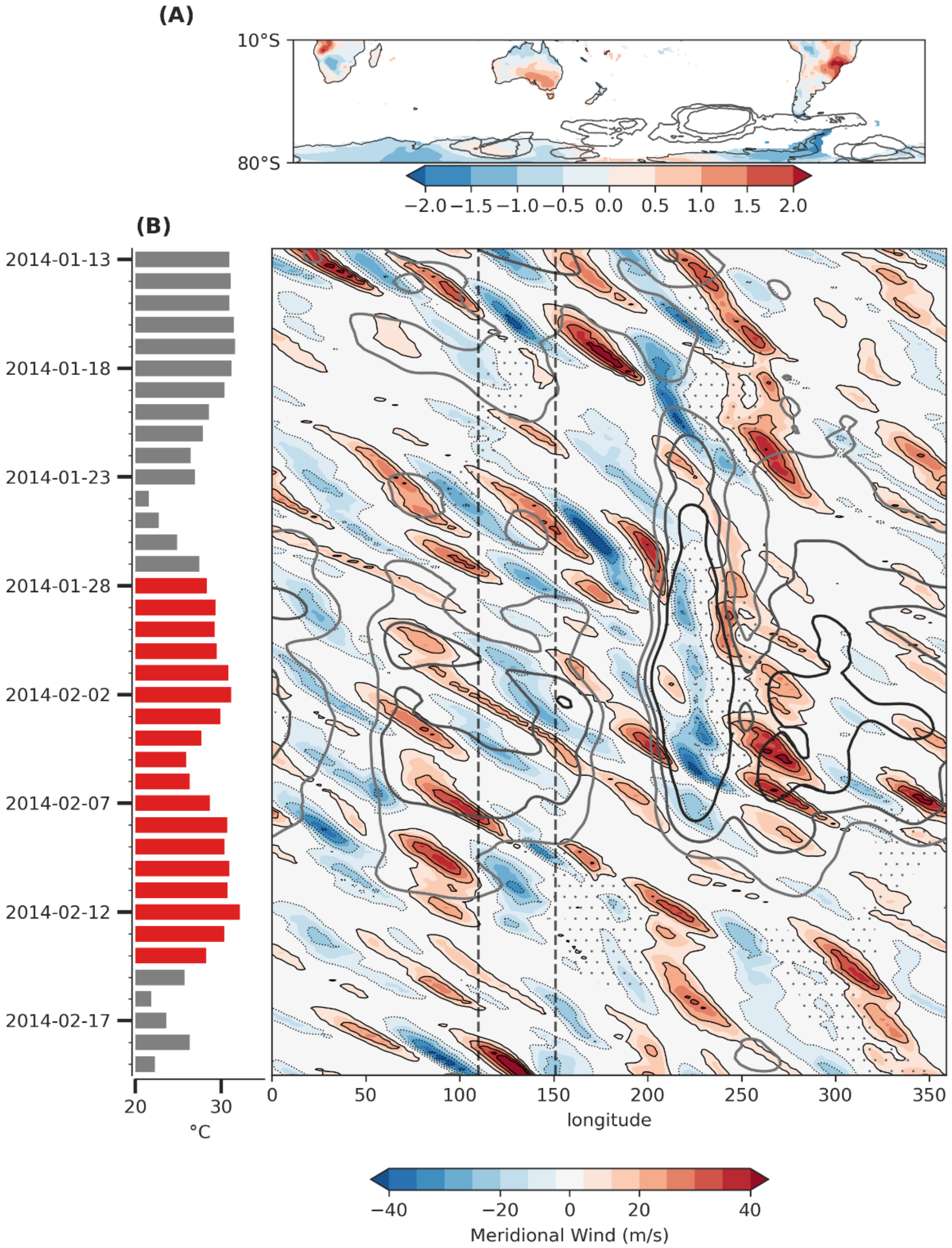

390 **Figure B1: Same as in Fig. 4 but for January 2014 SEA heatwave.**

Appendix C: Occurrence of High R_{SEA} on SEA heatwave days

	Days (DJF)	High R_{SEA} (days)
SEA heatwave days (SEA HD)	458	67
SEA non-heatwave days	3062	285
Total	3520	352
Probability	$P_{heatwave} = 0.13$	P (SEA HD | High R_{SEA}) = 0.19

Table C1: Occurrence of High R_{SEA} on SEA heatwave days and the associated conditional probabilities of a heatwave given high R_{SEA}.

395 Appendix D: Relationship between blocks and RRWPs in the South Pacific and the Indian Ocean

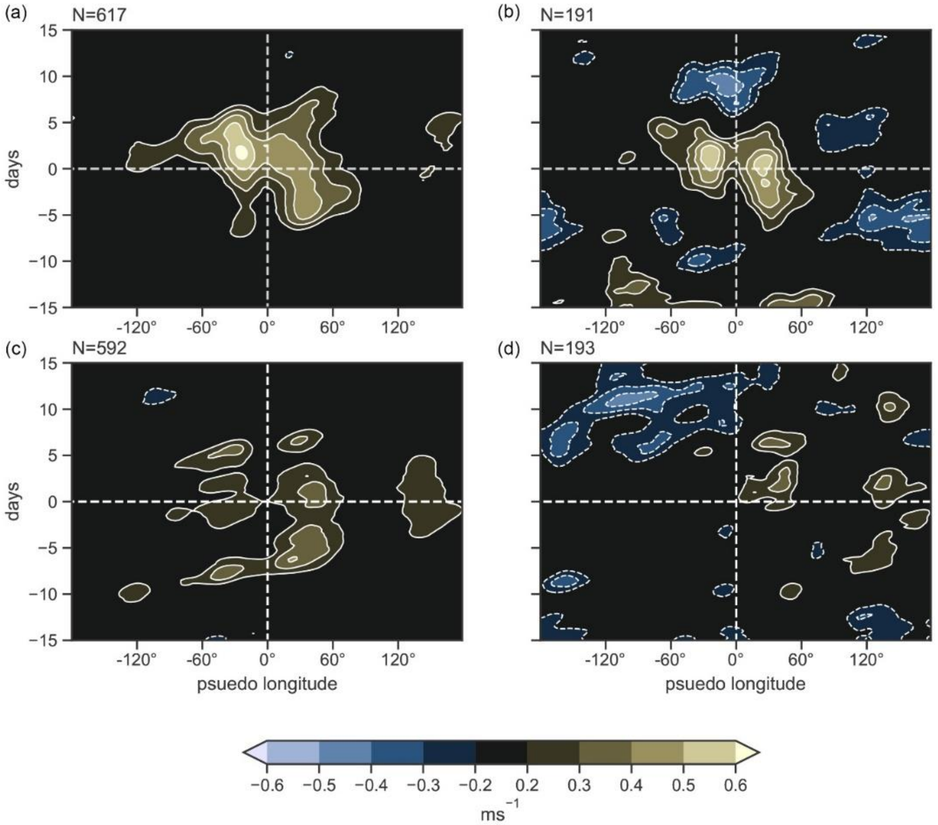

Figure D1: Time-lagged Hovmöller composites of R anomalies centred on the mean longitude and time of maximum amplitude of blocks located in Pacific Ocean (181–300° E, 30–80° S) in subplot (a) and (b), Indian Ocean (60–180° E, 30–80° S) in subplot (c) and (d). Left column includes blocks for all seasons and right shows for DJF. N denotes number of blocks for each category.

To further analyse the spatial distribution of RRWPs relative to blocks in the SH, we focus on two longitudinal subdomains that show a high blocking frequency in the DJF climatological mean (Fig. 11a): the South Pacific Ocean (230 – 310 °E), and the Indian Ocean (0 –90 ° E). We use time-lagged composite *R* anomalies with respect to the centroid of the blocks at the time of the maximum blocking amplitude in the two domains similar to Röthlisberger et al. (2019; see Fig. 12 in their paper). Here, *R* anomalies are calculated with respect to the day-of-year climatology.

In the Pacific Ocean, blocks coincide with positive *R* anomalies in a longitudinal band from ~60° upstream to ~60° downstream of the blocks (Fig. C1 a, b) from 5 to 8 days before the time of maximum blocking amplitude; this resembles a butterfly pattern, similar to blocks in the NH (Fig. 12, Röthlisberger et al., 2019). Similar to the NH, *R* anomalies in the Pacific Ocean are not high at the centroid of the block. This could be because the wavelength of the upper-level ridge associated with the block may be too wide to be captured by the *R* metric because the *R* metric only has contributions from k = 4 and higher. *R* anomalies are consistent for DJF and blocks for all seasons in the Pacific. In contrast, in the Indian Ocean, seasonal variation is seen in *R* anomalies (Fig. C1 c, d), where blocks located in DJF show *R* anomalies downstream of the centroid of the block only and possibly show weak association with RRWPs.

Code and data availability

Code for calculating *R* metric is available on GitHub (Ali and Röthlisberger, 2021). ACORN-SAT data is available at *http://www.bom.gov.au/climate/data/acorn-sat/#tabs=ACORN%E2%80%90SAT*. The ERA-I reanalysis dataset used can be downloaded from https://apps.ecmwf.int/datasets/data/interim-full-daily/levtype=pl/.

Author Contributions

SMA performed the formal analysis and wrote the first draft. All the authors contributed to the interpretation and discussion of the results and in review of the draft.

Competing Interests

The authors declare that they have no conflict of interest.

Acknowledgements

SMA is grateful for discussions with Alexandre Tuel and for the text editing by Simon Milligan. OM and SMA acknowledge Marco Rohrer for the blocking algorithm. The authors acknowledge the European Centre for Medium-Range Forecasts (ECMWF) for producing the ERA-I dataset and the Australian Bureau of Meteorology for producing ACORN-SAT dataset.

Funding information

SMA and OM were funded from the Swiss National Science Foundation grant number 178751. MR was funded from the INTEXseas project from the European Research Council under the European Union’s Horizon 2020 research and innovation program (Grant Agreement 787652). KK was partially supported by the NSF project NSF AGS-1934358.

References

Ali, M. and Röthlisberger, M.: avatar101/R-metric: (Version v1.1), Zenodo, https://doi.org/10.5281/zenodo.5742810, 2021.

Ali, S. M., Martius, O., and Röthlisberger, M.: Recurrent Rossby Wave Packets Modulate the Persistence of Dry and Wet Spells Across the Globe, Geophys. Res. Lett., 48, e2020GL091452, https://doi.org/https://doi.org/10.1029/2020GL091452, 2021.

Barriopedro, D., Fischer, E. M., Luterbacher, J., Trigo, R. M., and Garc\'\ia-Herrera, R.: The Hot Summer of 2010: Redrawing the Temperature Record Map of Europe, Science (80-.)., 332, 220–224, https://doi.org/10.1126/science.1201224, 2011.

Benjamini, Y. and Hochberg, Y.: Controlling the False Discovery Rate: A Practical and Powerful Approach to Multiple Testing, Source: Journal of the Royal Statistical Society. Series B (Methodological), 289–300 pp., 1995.

Black, E., Blackburn, M., Harrison, G., Hoskins, B., and Methven, J.: Factors contributing to the summer 2003 European heatwave, 59, 217–223, https://doi.org/10.1256/wea.74.04, 2004.

Coumou, D., Robinson, A., and Rahmstorf, S.: Global increase in record-breaking monthly-mean temperatures, Clim. Change, 118, 771–782, https://doi.org/10.1007/s10584-012-0668-1, 2013.

Davies, H. C.: Weather chains during the 2013/2014 winter and their significance for seasonal prediction, Nat. Geosci., https://doi.org/10.1038/ngeo2561, 2015.

Dee, D. P., Uppala, S. M., Simmons, A. J., Berrisford, P., Poli, P., Kobayashi, S., Andrae, U., Balmaseda, M. A., Balsamo, G., Bauer, P., Bechtold, P., Beljaars, A. C. M., van de Berg, L., Bidlot, J., Bormann, N., Delsol, C., Dragani, R., Fuentes, M., Geer, A. J., Haimberger, L., Healy, S. B., Hersbach, H., Hólm, E. V., Isaksen, L., Kållberg, P., Köhler, M., Matricardi, M., Mcnally, A. P., Monge-Sanz, B. M., Morcrette, J. J., Park, B. K., Peubey, C., de Rosnay, P., Tavolato, C., Thépaut, J. N., and Vitart, F.: The ERA-Interim reanalysis: Configuration and performance of the data assimilation system, Q. J. R. Meteorol. Soc., 137, 553–597, https://doi.org/10.1002/qj.828, 2011.

Drouard, M. and Woollings, T.: Contrasting Mechanisms of Summer Blocking Over Western Eurasia, Geophys. Res. Lett., 45, 12,040-12,048, https://doi.org/10.1029/2018GL079894, 2018.

Engel CB, Lane TP, Reeder MJ, Rezny M.: The meteorology of Black Saturday, Q. J. R.Meteorol. Soc. 139: 585–599, https://doi.org/10.1002/qj.1986, 2013.

Fragkoulidis, G., Wirth, V., Bossmann, P., and Fink, A. H.: Linking Northern Hemisphere temperature extremes to Rossby wave packets, Q. J. R. Meteorol. Soc., 144, 553–566, https://doi.org/10.1002/qj.3228, 2018.

Green, J. S. A.: The weather during July 1976: Some dynamical considerations of the drought. Weather, 32, 120-126, 1977.

Hoskins, B. J. and Sardeshmukh, P. D.: A Diagnostic Study of the Dynamics of the Northern Hemisphere Winter of 1985-86, Q. J. R.

Meteorol. Soc., 113, 759–778, https://doi.org/10.1002/qj.49711347705, 1987.

Hughes, L., Steffen, W., Mullins, G., Dean, A., Weisbrot, E., and Rice, M.: Summer of crisis, 2020.

Insurance Council Of Australia: INSURANCE COUNCIL OF AUSTRALIA, 2020.

Karoly D. J.: The recent bushfires and extreme heat wave in southeast Australia. Bull. Aust. Meteorol. Oceanogr. Soc., 22(1):10-3, 2009.

King, M.J., and Reeder, M.J.: Extreme heat events from an object viewpoint with application to south-east Australia. *Int J Climatol*.; 41: 2693– 2709, https://doi.org/10.1002/joc.6984, 2021.

Kautz, L.-A., Martius, O., Pfahl, S., Pinto, J. G., Ramos, A. M., Sousa, P. M., and Woollings, T.: Atmospheric blocking and weather extremes over the Euro-Atlantic sector – a review, Weather Clim. Dynam., 3, 305–336, https://doi.org/10.5194/wcd-3-305-2022, 2022.

Kornhuber, K., Petoukhov, V., Petri, S., Rahmstorf, S., and Coumou, D.: Evidence for wave resonance as a key mechanism for generating high-amplitude quasi-stationary waves in boreal summer, Clim. Dyn., 49, 1961–1979, https://doi.org/10.1007/s00382-016-3399-6, 2017.

Kornhuber, K., Coumou, D., Vogel, E., Lesk, C., Donges, J. F., Lehmann, J., and Horton, R. M.: Amplified Rossby waves enhance risk of concurrent heatwaves in major breadbasket regions, Nat. Clim. Chang., 10, 48–53, https://doi.org/10.1038/s41558-019-0637-z, 2020.

Martius, O., C. Schwierz, and H. C. Davies.: Tropopause-level waveguides, J. Atmos.Sci., 67, 866–879, https://doi.org/10.1175/2009JAS2995.1, 2010.

Martius, O., Wehrli, K., & Rohrer, M.: Local and Remote Atmospheric Responses to Soil Moisture Anomalies in Australia, Journal of Climate, 34(22), 9115-9131, https://doi.org/10.1175/JCLI-D-21-0130.1, 2021.

Masson-Delmotte, V., P. Zhai, A. Pirani, S. L., Connors, C. Péan, S. Berger, N. Caud, Y. Chen, L. Goldfarb, M.I. Gomis, M. Huang, K. Leitzell, E. Lonnoy, J. B. R., and Matthews, T.K. Maycock, T. Waterfield, O. Yelekçi, R. Yu, and B. Z. (eds. .: IPCC, 2021: Climate Change 2021: The Physical Science Basis. Contribution of Working Group I to the Sixth Assessment Report of the Intergovernmental Panel on Climate Change, https://www.ipcc.ch/report/ar6/wg1/#FullReport, 2021.

National Climate Centre (2004) Eastern Australia experiences record February heatwave. Bull. Aust. Meteorol. Oceanogr Soc. 17:27–29

O'Brien, L. and Reeder, M. J.: Southern Hemisphere summertime Rossby waves and weather in the Australian region, Q. J. R. Meteorol. Soc., 143, 2374–2388, https://doi.org/10.1002/qj.3090, 2017.

Parker, T., Berry, G. J., Reeder, M. J., and Nicholls, N.: Modes of climate variability and heat waves in Victoria, southeastern Australia, Geophys. Res. Lett., 41, 6926–6934, https://doi.org/10.1002/2014GL061736, 2014a.

Parker, T., Berry, G. J., and Reeder, M. J.: The Structure and Evolution of Heat Waves in Southeastern Australia, J. Clim., 27, 5768–5785, https://doi.org/10.1175/JCLI-D-13-00740.1, 2014b.

Parker, T., Quinting, J., and Reeder, M.: The synoptic-dynamics of summertime heatwaves in the Sydney area (Australia), J. South.

Hemisph. Earth Syst. Sci., 69, 116, https://doi.org/10.1071/es19004, 2019.

Pelly, J. L., & Hoskins, B. J.: A New Perspective on Blocking, Journal of the Atmospheric Sciences, 60(5), 743-755, https://doi.org/10.1175/1520-0469(2003)060<0743:ANPOB>2.0.CO;2 , 2003.

Perkins-Kirkpatrick, S. E. and Lewis, S. C.: Increasing trends in regional heatwaves, Nat. Commun., 11, 1–8, 2020.

Petoukhov, V., Rahmstorf, S., Petri, S., and Schellnhuber, H. J.: Quasiresonant amplification of planetary waves and recent Northern Hemisphere weather extremes, Proc. Natl. Acad. Sci. U. S. A., 110, 5336–5341, https://doi.org/10.1073/pnas.1222000110, 2013.

Pfahl, S. and Wernli, H.: Quantifying the relevance of atmospheric blocking for co-located temperature extremes in the Northern Hemisphere on (sub-)daily time scales, Geophys. Res. Lett., 39, 1–6, https://doi.org/10.1029/2012GL052261, 2012.

Quandt, L.-A., Keller, J. H., Martius, O., and Jones, S. C.: Forecast variability of the blocking system over Russia in summer 2010 and its impact on surface conditions, Weather Forecast., 32, 61–82, 2017.

Quinting, J. F., and Reeder, M. J.,: Southeastern Australian Heat Waves from a Trajectory Viewpoint, Mon. Weather Rev., 145, 4109–4125, https://doi.org/10.1175/MWR-D-17-0165.1, 2017.

Risbey, J. S., O'Kane, T. J., Monselesan, D. P., Franzke, C. L. E., and Horenko, I. On the dynamics of Austral heat waves. *Journ. of Geophys. Res.: Atmos.*, 123, 38– 57. https://doi.org/10.1002/2017JD027222, 2018.

Rohrer, M., Brönnimann, S., Martius, O., Raible, C. C., Wild, M., and Compo, G. P.: Representation of extratropical cyclones, blocking anticyclones, and alpine circulation types in multiple reanalyses and model simulations, J. Clim., 31, 3009–3031, https://doi.org/10.1175/JCLI-D-17-0350.1, 2018.

Röthlisberger, M., Frossard, L., Bosart, L. F., Keyser, D., and Martius, O.: Recurrent synoptic-scale Rossby wave patterns and their effect on the persistence of cold and hot spells, J. Clim., 32, 3207–3226, https://doi.org/10.1175/JCLI-D-18-0664.1, 2019.

Schneidereit, A., Schubert, S., Vargin, P., Lunkeit, F., Zhu, X., Peters, D. H. W., and Fraedrich, K.: Large-Scale Flow and the Long-Lasting Blocking High over Russia: Summer 2010, Mon. Weather Rev., 140, 2967–2981, https://doi.org/10.1175/MWR-D-11-00249.1, 2012.

Schwierz, C., Croci-Maspoli, M., and Davies, H. C.: Perspicacious indicators of atmospheric blocking, Geophys. Res. Lett., 31, 6, https://doi.org/10.1029/2003gl019341, 2004.

Seneviratne, S.I., Corti, T., Davin, E.L., Hirschi, M., Jaeger, E.B., Lehner, I., Orlowsky, B. and Teuling, A.J.: Investigating soil moisture–climate interactions in a changing climate: A review. Earth-Science Reviews, 99(3-4), pp.125-161., 2010.

Shepherd, T. G.: Atmospheric circulation as a source of uncertainty in climate change projections, Nat. Geosci., 7, 703–708, https://doi.org/10.1038/NGEO2253, 2014.

Shutts, G. J.: The propagation of eddies in diffluent jetstreams: Eddy vorticity forcing of ‘blocking’ flow fields, Q. J. R. Meteorol. Soc., https://doi.org/10.1002/qj.49710946204, 1983.

Sousa, P. M., D. Barriopedro, R. García-Herrera, T. Woollings, and R. M. Trigo: A new combined detection algorithm for blocking and subtropical ridges. J. Clim, 34, 18, 7735-7758, https://doi.org/10.1175/JCLI-D-20-0658.1, 2021.

Teng, H., Branstator, G., Meehl, G. A., and Washington, W. M.: Projected intensification of subseasonal temperature variability and heat waves in the Great Plains, Geophys. Res. Lett., 43, 2165–2173, https://doi.org/https://doi.org/10.1002/2015GL067574, 2016.

Trigo, R. M., Trigo, I. F., DaCamara, C. C., and Osborn, T. J.: Climate impact of the European winter blocking episodes from the NCEP/NCAR Reanalyses, Clim. Dyn., 23, 17–28, https://doi.org/10.1007/s00382-004-0410-4, 2004.

VBRC: Final report of the Victorian Bushfires Royal Commission. [Available online at http://www.royalcommission.vic.gov.au/Commission-Reports.], 2010.

Wehrli, K., Guillod, B. P., Hauser, M., Leclair, M., and Seneviratne, S. I.: Identifying Key Driving Processes of Major Recent Heat Waves, J. Geophys. Res. Atmos., 124, 11746–11765, https://doi.org/https://doi.org/10.1029/2019JD030635, 2019.

Wernli, H. and Schwierz, C.: Surface cyclones in the ERA-40 dataset (1958-2001). Part I: Novel identification method and global climatology, J. Atmos. Sci., 63, 2486–2507, https://doi.org/10.1175/JAS3766.1, 2006.

White, R. H., Kornhuber, K., Martius, O., and Wirth, V.: From Atmospheric Waves to Heatwaves: A Waveguide Perspective for Understanding and Predicting Concurrent, Persistent and Extreme Extratropical Weather, Bull. Am. Meteorol. Soc., 1–35, https://doi.org/10.1175/BAMS-D-21-0170.1, 2021.

Wilks, D. S.: “The stippling shows statistically significant grid points”: How research results are routinely overstated and overinterpreted, and what to do about it, https://doi.org/10.1175/BAMS-D-15-00267.1, 2016.

Wirth, V., Riemer, M., Chang, E. K. M., and Martius, O.: Rossby Wave Packets on the Midlatitude Waveguide — A Review, Mon. Weather Rev., MWR-D-16-0483.1, https://doi.org/10.1175/MWR-D-16-0483.1, 2018.

Zimin, A. V., Szunyogh, I., Patil, D. J., Hunt, B. R., and Ott, E.: Extracting Envelopes of Rossby Wave Packets, Mon. Weather Rev., https://doi.org/10.1175/1520-0493(2003)131<1011:EEORWP>2.0.CO;2, 2003.

Wolf, G., Brayshaw, D.J., Klingaman, N.P. and Czaja, A.: Quasi-stationary waves and their impact on European weather and extreme events. Quarterly Journal of the Royal Meteorological Society, 144(717), pp.2431-2448, 2018.